The Journal of Chemical Physics

Theory of the effect of external stress on the activated dynamics and transport of dilute penetrants in supercooled liquids and glasses

Cite as: J. Chem. Phys. **155**, 054505 (2021); https://doi.org/10.1063/5.0056920
Submitted: 15 May 2021 • Accepted: 19 July 2021 • Published Online: 04 August 2021

Baicheng Mei and Kenneth S. Schweizer

The Journal of Chemical Physics ARTICLE scitation.org/journal/jcp

Theory of the effect of external stress on the activated dynamics and transport of dilute penetrants in supercooled liquids and glasses

Cite as: J. Chem. Phys. 155, 054505 (2021); doi: 10.1063/5.0056920
Submitted: 15 May 2021 • Accepted: 19 July 2021 •
Published Online: 4 August 2021

Baicheng Mei[1,2] and Kenneth S. Schweizer[1,2,3,4,a)]

AFFILIATIONS

[1] Department of Materials Science, University of Illinois, Urbana, Illinois 61801, USA
[2] Materials Research Laboratory, University of Illinois, Urbana, Illinois 61801, USA
[3] Department of Chemistry, University of Illinois, Urbana, Illinois 61801, USA
[4] Department of Chemical and Biomolecular Engineering, University of Illinois, Urbana, Illinois 61801, USA

[a)] Author to whom correspondence should be addressed: kschweiz@illinois.edu

ABSTRACT

We generalize the self-consistent cooperative hopping theory for a dilute spherical penetrant or tracer activated dynamics in dense metastable hard sphere fluids and glasses to address the effect of external stress, the consequences of which are systematically established as a function of matrix packing fraction and penetrant-to-matrix size ratio. All relaxation processes speed up under stress, but the difference between the penetrant and matrix hopping (alpha relaxation) times decreases significantly with stress corresponding to less time scale decoupling. A dynamic crossover occurs at a critical "slaving onset" stress beyond which the matrix activated hopping relaxation time controls the penetrant hopping time. This characteristic stress increases (decreases) exponentially with packing fraction (size ratio) and can be well below the absolute yield stress of the matrix. Below the slaving onset, the penetrant hopping time is predicted to vary exponentially with stress, differing from the power law dependence of the pure matrix alpha time due to system-specificity of the stress-induced changes in the penetrant local cage and elastic barriers. An exponential growth of the penetrant alpha relaxation time with size ratio under stress is predicted, and at a fixed matrix packing fraction, the exponential relation between penetrant hopping time and stress for different size ratios can be collapsed onto a master curve. Direct connections between the short- and long-time activated penetrant dynamics and between the penetrant (or matrix) alpha relaxation time and matrix thermodynamic dimensionless compressibility are also predicted. The presented results should be testable in future experiments and simulations.

I. INTRODUCTION

The activated dynamics and transport of dilute atomic and molecular "penetrants" or "tracers" in glass-forming viscous liquids and glasses[1–11] and their dense nanoparticle/colloidal suspension analogs[12–17] have attracted increasing attention. The problem is of fundamental physics interest and is also relevant to many applications such as membrane separations,[5–8] suppression of gas permeation in coatings,[6,7] self-healing based on controlled release of reactive molecules from microcapsules,[18,19] and ion and solvent transport in biological and polymeric materials.[5,20] Experimental, theoretical, and simulation studies of penetrant transport have almost always been under mechanically quiescent conditions.[3,6,20–36] Here, we construct a microscopic theory for how macroscopic deformation affects this problem.

Existing theories for quiescent penetrant dynamics are almost entirely phenomenological, typically built around the difficult to quantify idea of "free volume."[5,8,20,24,36] Recently, the microscopic, force-level, self-consistent cooperative hopping (SCCH) theory[37,38] was constructed by Zhang and Schweizer to predict activated penetrant dynamics in dense fluids and glasses. It builds on the Elastically Collective Nonlinear Langevin Equation (ECNLE)

theory of the pure matrix alpha relaxation process,[39,40] where caging enters via a dynamic free energy coupled with longer-range collective elasticity. The physical ideas of SCCH theory bear some similarity with classic problems in solid state physics, e.g., small polaron transport[41] and interstitial diffusion in crystals,[42] where local steric obstruction and correlated longer-range collective elasticity of the medium (phonons) play crucial roles. Notable predictions of SCCH theory[38,43] in the dilute penetrant limit include an exponential relationship between the penetrant alpha time and its size, a power law relationship between the penetrant size and the transient localization length, and a linear correlation between the logarithm of the penetrant alpha time and the matrix inverse dimensionless compressibility. The former two predictions have been recently shown[43] to be in good agreement with simulations and experiments.

Here, SCCH theory is extended to address how a macroscopic applied stress changes penetrant dynamics. We build on the recent progress[44] of Ghosh and Schweizer for various aspects of the nonlinear rheology of the pure matrix system in the ECNLE theory framework (in its constant stress creep deformation realization). Stress affects the penetrant and matrix dynamic free energies in different, but coupled, ways, depending strongly on the size asymmetry ratio. A foundational aspect of the SCCH theory[38,43] is a direct connection between activated dynamics and equilibrium pair correlations. Here, we employ an accurate integral equation theory based on the modified-Verlet (MV) closure[45,46] to determine the required structural inputs.

Section II reviews the relevant theoretical background for the pure matrix fluid. Section III formulates the extension of the SCCH approach for penetrant dynamics to include external stress. This then allows us to concretely pose in Sec. III B the key new physical questions we address in Secs. IV–VI. Section IV presents predictions for how stress changes the penetrant hopping time, including the crossover from a regime where the penetrant and matrix activated hopping times are decoupled to when penetrant hopping is fully "slaved" to the matrix hopping relaxation process. The quantitative dependence on the matrix packing fraction and size ratio of the stress-dependent degree of decoupling in the pre-slaving regime is analyzed in Sec. V. Section VI establishes detailed predictions for the absolute magnitude of the stress-dependent penetrant alpha relaxation time and transient localization length, connection between short- and long-time penetrant dynamics, and a power law correlation between the penetrant (or matrix) alpha relaxation time and a specific matrix thermodynamic property. This article concludes in Sec. VII with a summary and a brief discussion of future opportunities to treat more complex systems.

II. THEORETICAL BACKGROUND: ECNLE THEORY FOR THE PURE MATRIX SYSTEM UNDER QUIESCENT CONDITIONS AND WITH EXTERNAL STRESS

All the required theoretical methods under *both* quiescent[39,40,47] and constant stress[44] conditions for the *one-component* hard sphere system studied here have been described in detail previously. We, thus, only recall the results required for our present work. Readers familiar with the one-component ECNLE theory can proceed directly to Sec. III.

ECNLE theory for one-component fluids[39,40,47] enters SCCH theory,[38,43] since in the infinitely dilute penetrant limit of present interest, the matrix dynamics is taken to be unperturbed. The displacement-dependent matrix dynamic free energy, $\beta F_{\rm dyn}(r)$, is the key quantity, which in the absence of external force is[48,49]

$$\beta F_{\rm dyn}(r) = -3\,\ln(r/d_{\rm m}) - \int \frac{d\mathbf{q}}{(2\pi)^3}\frac{\rho C^2(q)S(q)}{1+S^{-1}(q)} e^{-q^2r^2(1+S^{-1}(q))/6}, \tag{1}$$

where $\beta = 1/k_{\rm B}T$ is the inverse thermal energy, $k_{\rm B}$ is Boltzmann's constant, T is temperature, $r(t)$ is the particle scalar displacement at time t from its initial position, $d_{\rm m}$ is the matrix particle diameter, ρ is the fluid number density, $S(q)$ is the structure factor, and $C(q) = \rho^{-1}[1 - S^{-1}(q)]$ is the direct correlation function. The required static pair correlation functions are computed using the Ornstein–Zernike (OZ) integral equation,[50] which in Fourier space is

$$h(q) = C(q) + \rho C(q)h(q) = C(q)S(q), \tag{2}$$

where $h(q)$ is the Fourier transform of $h(r) = g(r) - 1$ with $g(r)$ the radial distribution function. The MV closure,[45,46,51–53] which is very accurate at the relevant high packing fractions, is employed. For the two-component mixture of hard spheres[46] studied in the present work, it can be written as

$$b_{ij}^{\rm MV}(r) = \frac{-a_1\lambda_{ij}^2(r)}{1+a_2|\lambda_{ij}(r)|}, \tag{3}$$

where $\lambda_{ij}(r) = h_{ij}(r) - c_{ij}(r)$ with i and j labeling the particle type (matrix, m; penetrant, p), $a_1 = 0.5$, and $a_2 = 0.8$. The integral equations are numerically solved using standard methods.[50] The second term in Eq. (1) corresponds to an effective dynamic potential due to interparticle forces, which favors transient localization and caging. In quiescent systems, the stochastic trajectory of a tagged (spherical) particle in the overdamped limit obeys[48,49]

$$-\xi_{\rm s}\frac{dr(t)}{dt} - \frac{\partial}{\partial r}F_{\rm dyn}(r(t)) + \delta\eta(t) = 0, \tag{4}$$

where $\xi_{\rm s}$ quantifies the short-time/distance non-activated relaxation process[54] and $\delta\eta$ is the corresponding white noise random force that satisfies $\langle\delta\eta(t)\delta\eta(0)\rangle = 2\beta^{-1}\xi_{\rm s}\delta(t)$.

If a constant external force, f, is applied to every particle, the dynamic free energy, ignoring force-induced changes in the equilibrium structure on the relevant *local* scale, is[55,56]

$$\beta F_{\rm dyn}(r) = -3\,\ln(r/d_{\rm m}) - \int \frac{d\mathbf{q}}{(2\pi)^3}\frac{\rho C^2(q)S(q)}{1+S^{-1}(q)} e^{-q^2r^2(1+S^{-1}(q))/6} - \beta f r. \tag{5}$$

External macroscopic stress, σ, enters in a microrheological spirit as[44,56]

$$f = d_{\rm m}^2\sigma/\phi^{2/3}. \tag{6}$$

In the absence of noise, or if the dynamic free energy is approximated by a harmonic form, Eqs. (4) and (5) reduce to the naïve mode

coupling theory (NMCT) self-consistent equation for the long-time limit of the particle mean square displacement or localization length,[49,56,57]

$$r_{\rm loc}^{-2} = \frac{1}{9}\int \frac{d\mathbf{q}}{(2\pi)^3} q^2 \rho C^2(q) S(q) e^{-q^2 r_{\rm loc}^2 (1+S^{-1}(q))/6} - \frac{\beta f}{3 r_{\rm loc}}. \quad (7)$$

For quiescent hard sphere fluids, an ideal NMCT transition occurs at a packing fraction of $\phi \sim 0.43$.[49] The external force enhances particle motion and shifts the ideal transition to a higher packing fraction, beyond which the dynamic localization length becomes applied force dependent.

The ideal NMCT transition is a dynamic crossover, beyond which a transiently localized state and a barrier emerge in the dynamic free energy.[48,49] For $\phi > 0.43$ under quiescent conditions, the barrier is finite for all packing fractions below a random close packing value of $\phi \sim 0.64$. The dynamic confinement is characterized by a finite maximum cage restoring force, $f_{\rm max}$, at a displacement R^*.[48,49] Thus, the application of an external force of magnitude $f = f_{\rm y} = f_{\rm max}$ (or "absolute yield stress," $\sigma_{\rm y}$) destroys the localized form corresponding to a mechanically induced crossover from a solid-like to a liquid-like (no barrier) form of the dynamic free energy.[44,56]

Two example dynamic free energies are shown in Fig. 1(a). Key length scales are a minimum at $r_{\rm loc}$ (transient localization length), a maximum at the barrier location, $r_{\rm B}$, an inflection point (location of the maximum restoring force) at R^*, and a microscopic jump distance of $\Delta r \equiv r_{\rm B} - r_{\rm loc}$. Key energy scales are the local cage barrier ($F_{\rm B}$), $f_{\rm max}$, and the positive curvatures of the dynamic free energy at its minimum (K_0) and maximum ($-K_{\rm B}$). With increasing external force, all length and energy scales decrease with the exception of $r_{\rm loc}$, which increases and ultimately merges with $r_{\rm B}$ at $f = f_{\rm y}$.

Since hopping is predicted to involve a relatively large particle displacement ($\Delta r \approx 0.2 d_{\rm m}$–$0.4 d_{\rm m}$), Mirigian and Schweizer argued that a small amount of extra space (cage expansion) beyond the equilibrium cage scale is required to allow activated motion on the cage scale,[39,40] a physical idea motivated by the phenomenological "shoving model" of Dyre.[58–60] Including this physics microscopically in Nonlinear Langevin Equation (NLE) theory defines ECNLE theory and introduces the collective elastic fluctuation of particles outside the cage of radius $r_{\rm cage}$ [defined from the first minimum of $g(r)$] as a crucial component of structural relaxation. The elastic barrier becomes important at sufficiently low (high) temperature (packing fraction) and follows from summing over elastic displacements of all particles outside the cage, thereby yielding[40]

$$\beta F_{\rm el} \approx 2\pi\rho r_{\rm cage}^3 \Delta r_{\rm eff}^2 K_0, \quad (8)$$

where $\Delta r_{\rm eff} \approx 3\Delta r^2/32 r_{\rm cage}$. The elastic barrier is determined mainly by[40,47] the fourth power of the particle jump distance, Δr,[4] and the localized state spring constant, $K_0 = 3k_{\rm B}T/r_{\rm loc}^2$. The alpha relaxation event is then a coupled local–nonlocal process involving coordinated cage scale hopping and a long-range elastic fluctuation, with the total barrier equal to the sum of the local cage and collective elastic contributions. Both barriers decrease with an external force,[44] with the elastic one decreasing *much* faster due to its sensitivity to both the jump distance and K_0.

The mean alpha relaxation time is estimated as

$$\tau_\alpha = \tau_{\rm s} + \tau_{\rm hop}, \quad (9a)$$

where $\tau_{\rm s}$ is the very local and fast (taken to be stress independent) non-activated process relaxation time, which for a Newtonian hard sphere fluid is[40,47]

$$\tau_{\rm s} = \tau_{\rm E}\left[1 + \frac{1}{6\pi^2}\int_0^\infty dq q^2 \frac{\rho C^2(q) S(q)}{1 + n(q)/S(q)}\right], \quad \tau_{\rm E} = \tau_0 g(d_{\rm m}), \quad \tau_0 = 16\phi d_{\rm m}\sqrt{\beta M/\pi}, \quad (9b)$$

where M is the particle mass, $g(d_{\rm m})$ is the contact value of $g(r)$, and $1/n(q) = 1 - j_0(q) + 2j_2(q)$ with $j_\alpha(q)$ being the Bessel function of order α. The mean first passage or barrier hopping time is computed using Kramers theory[61,62] as

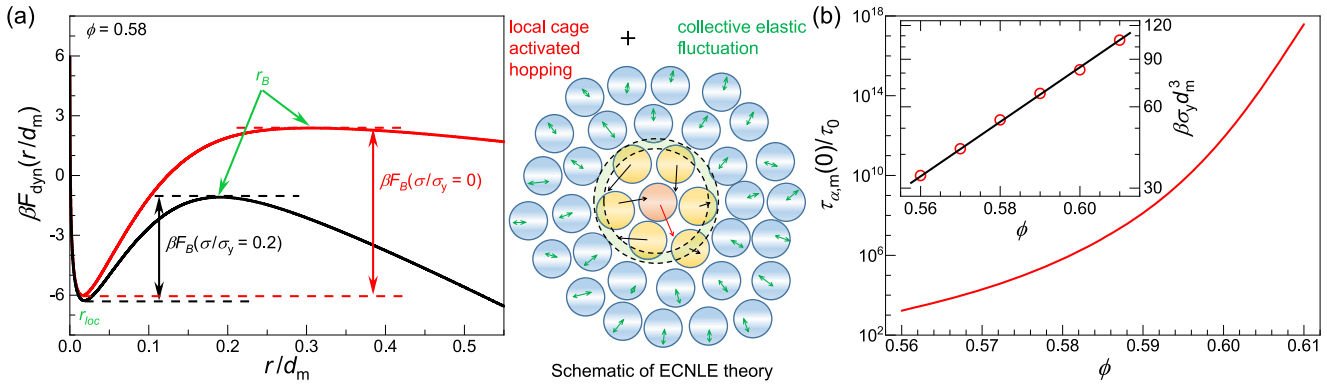

FIG. 1. (a): Dynamic free energy (in units of thermal energy) of the hard sphere fluid under quiescent and stressed ($\sigma/\sigma_{\rm y} = 0.2$) conditions vs scaled particle displacement at $\phi = 0.58$; important length and energy scales defined in the text are indicated. Right panel: sketch of the physical ideas of ECNLE theory. (b) Main panel shows the mean alpha relaxation time (units of the elementary time scale τ_0) as a function of packing fraction. Inset: exponential relation between the dimensionless maximum cage restoring force under quiescent conditions (equal to within units to the absolute yield stress $\beta\sigma_{\rm y} d_{\rm m}^3$) and packing fraction.

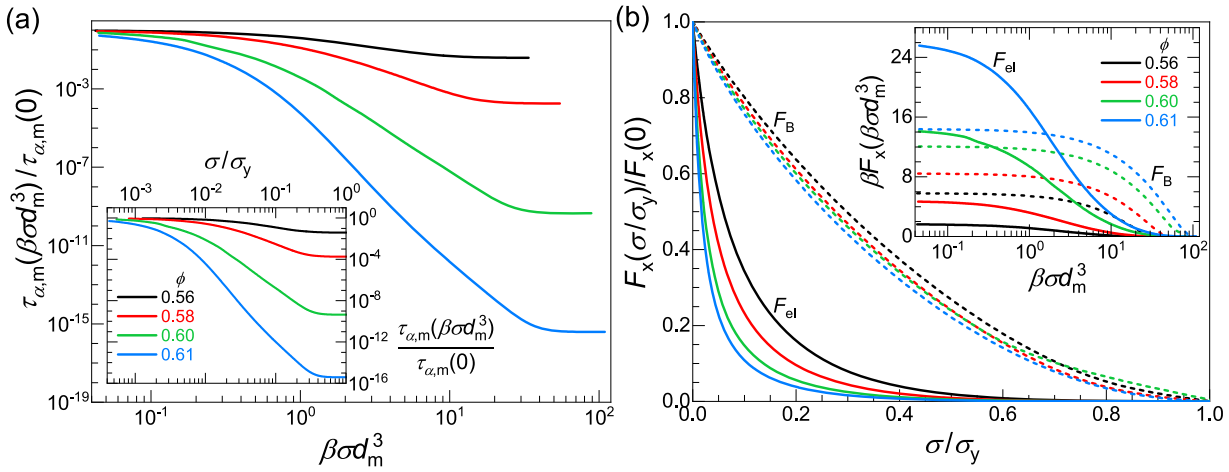

FIG. 2. (a) Double log plot of the alpha time of the hard sphere fluid normalized by its zero-stress quiescent value as a function of dimensionless stress (main) and stress scaled by its absolute yield value σ/σ_y (inset) at several high packing fractions. For quiescent viscous liquids (elementary object size ~1 nm), these packing fractions correspond to Ref. 43: (i) where elasticity just begins to become important ($\phi = 0.56$, $\tau_\alpha \sim 1.6$ ns, $F_{el}/F_B \sim 0.27$, $\beta F_{el} \sim 1.57$), (ii) an intermediate packing fraction ($\phi = 0.58$, $\tau_\alpha \sim 359$ ns, $F_{el}/F_B \sim 0.53$, $\beta F_{el} \sim 4.45$), (iii) a very high packing fraction ($\phi = 0.60$ $\tau_\alpha \sim 0.25$ s, $F_{el}/F_B \sim 1.11$, $\beta F_{el} \sim 13.46$), and (iv) slightly beyond the kinetic glass transition ($\phi = 0.61$ $\tau_\alpha \sim 10^5$ s, $F_{el}/F_B \sim 1.68$, $\beta F_{el} \sim 24.25$). (b) Main: elastic (solid) and local cage (short-dashed) barriers scaled by their zero-stress analogs as a function of σ/σ_y at various packing fractions identical to those in (a). Inset: same results as those in the main frame but with both axes not normalized as in the main frame.

$$\tau_{hop} = \frac{2\tau_s e^{\beta F_{el}}}{d_m^2} \int_{r_{loc}}^{r_{loc}+\Delta r} dr e^{\beta F_{dyn}(r)} \int_{r_{loc}}^{r} dr' e^{-\beta F_{dyn}(r')}$$
$$= \tau_s \frac{2\pi}{\sqrt{K_0 K_B}} e^{\beta(F_B+F_{el})}. \quad (10)$$

The second expression is very accurate beyond a cage barrier of ~1–2k_BT.

The main frame of Fig. 1(b) shows alpha time calculations as a function of packing fraction under quiescent conditions. Collective elastic physics is unimportant when $\phi = 0.44$–0.56, followed by a crossover at $\phi = 0.56$ (where $\beta F_{el} \sim 1.5$), beyond which elasticity effects increasingly dominate for $\phi = 0.56$–0.60, leading to kinetic vitrification at $\phi \sim 0.605$. The latter is deduced from the criterion that $\tau_\alpha/\tau_0 = 10^{14}$, corresponding to 100 s for a thermal liquid with $\tau_0 = 1$ ps. As the external force or stress increases, all the trapping features of the dynamic free energy are reduced. Eventually, the localized state and barrier merge and disappear thereby defining the "absolute yield stress," which in dimensionless units is $\beta\sigma_y d_m^3$.

The results for the stress-induced barrier and alpha time reductions are shown in Fig. 2. The alpha time decreases as an effective power law function beginning at very low values of dimensionless stress, a behavior that becomes more well-defined as the packing fraction increases. The analogous stress normalized plot is shown in the inset of Fig. 2(a). The high stress plateau indicates that the alpha time approaches the corresponding non-activated short relaxation time, τ_s, at reduced stresses of $\sigma/\sigma_y \sim 0.3$ (i.e., $\tau_s \gg \tau_{hop}$, $\tau_\alpha \equiv \tau_s + \tau_{hop} \approx \tau_s$), which occurs *well below* the absolute yield point where the total barrier vanishes ($\tau_{hop} \to 0$). This behavior is a consequence of the very high sensitivity of the elastic barrier reduction to stress,[44] resulting in the inequality $\tau_s \gg \tau_{hop}$ not being identical to $\tau_{hop} \to 0$ literally, as illustrated in Fig. 2(b). Thus, the emergence of a plateau in Fig. 2(a) can be viewed as defining a practical yield stress σ_y', which is always smaller than the absolute yield stress σ_y where the barrier rigorously vanishes. The physical picture is, thus, for stresses beyond σ_y' but below σ_y, although hopping over low barriers still exists, it does not play a crucial role in the total alpha relaxation time as defined in Eq. (9a). Of course, beyond σ_y the alpha relaxation process literally has no activated component (zero barrier). Given in ECNLE theory that the logarithm of the alpha time reflects the sum of local cage and collective elastic barriers (when the short-time non-activated process contribution is unimportant), the power law in the stress regime shown in Fig. 2(a) has a somewhat subtle origin since it does *not* simply reflect the stress dependence of the individual local cage or elastic barrier, as demonstrated in the inset of Fig. 2(b). Rather, the extended power law behavior in Fig. 2(a) reflects the fact that, although the local cage barrier decreases modestly compared to the strong decrease in its elastic counterpart at low stresses, there is a weak compensation effect between the local cage and elastic barriers. Nevertheless, at high packing fractions, where elasticity is very important in equilibrium, the decrease in the alpha time in the low stress regime is mainly determined[44] by the elastic barrier. This effective power law between the *matrix* alpha time and stress differs from the linear relationship between the *penetrant* alpha time and stress as analyzed below. A more detailed discussion of the influence of external stress on the matrix relaxation can be found in Ref. 44.

III. EXTENSION OF SCCH THEORY TO INCLUDE EXTERNAL FORCE

A. Formulation in the dilute penetrant limit

SCCH theory under quiescent conditions[38,43] has been discussed in detail previously. Here, we briefly recall its basic ideas and

then present the generalization to include an external stress following the same approach as for the pure matrix system reviewed in Sec. II.

In the dilute penetrant (diameter d_p) limit, the analog of Eq. (4) for the instantaneous penetrant displacement (trajectory), r_p, from its initial position is[38,43]

$$-\xi_{s,p}\frac{dr_p}{dt} - \frac{\partial}{\partial r}F_{dyn,p} + \delta\eta_p = 0, \tag{11}$$

where $\delta\eta_p$ is the white noise random force corresponding to $\xi_{s,p} = k_B T\tau_{s,p}/d_p^2$ associated with the penetrant–matrix interactions (here collisions).[43,54,63,64] Repeating the standard NMCT analysis[49,56] yields the self-consistent equation for the penetrant localization length under an external force f_p,

$$r_{loc,p}^{-2} = \frac{1}{9}\int \frac{d\mathbf{q}}{(2\pi)^3} q^2\rho C_{mp}^2(q)S_{mm}(q)e^{-q^2r_{loc,p}^2/6} \times e^{-q^2r_{loc,m}^2/6S_{mm}(q)} - \frac{\beta f_p}{3r_{loc,p}}. \tag{12}$$

Information about the matrix static structure factor, penetrant–matrix pair correlation function, and matrix dynamic localization length all is entered into Eq. (12). The required penetrant–matrix pair correlation function is computed using the OZ integral equation $h_{mp}(q) = C_{mp}(q)S_{mm}(q)$ with the MV closure of Eq. (3).

Based on Eq. (12), the penetrant dynamic free energy in the presence of an external force on it, f_p, obeys[38,43]

$$\frac{\partial\beta F_{dyn,p}(r_p,r_m)}{\partial r_p} = -\frac{3}{r_p} + \frac{r_p}{3}\int \frac{d\mathbf{q}}{(2\pi)^3} q^2\rho C_{mp}^2(q)S_{mm}(q) \times e^{-q^2r_p^2/6}e^{-q^2r_m^2/6S_{mm}(q)} - \beta f_p. \tag{13}$$

Setting this derivative to zero yields the corresponding NMCT localization equation of Eq. (12). In general, the penetrant dynamic free energy depends on *both* the displacement dynamical variables, r_p and r_m, reflecting the coupling of penetrant motion to matrix displacements *at* the trajectory level. The latter complicated aspect is approximately handled in SCCH theory[38,43] (see Fig. 3) by introducing a cooperative displacement variable quantified by a single "coupling" parameter, γ, which quantifies the slower (matrix) and faster (penetrant) displacements as $r_m(\gamma) = r_{loc,m} + (r_p - r_{loc,p})/\gamma$. Substituting it into Eq. (13), the penetrant dynamic free energy follows via numerical integration. The external force on a penetrant due to a macroscopic stress is determined in the same microrheological spirit as done for the pure matrix case as

$$f_p = d_p^2\sigma/\phi^{2/3}, \tag{14}$$

which differs from the microscopic force on a matrix particle, f_m, only due to the different microscopic cross sectional area factor. The effect of macroscopic external stress then enters in a microscopic force manner at the level of the matrix and penetrant dynamic free energies, as indicated in Fig. 3.

The theory is rendered predictive based on the enforcement of the *temporal self-consistent* condition $\tau_{hop,p}[\Delta r_p(\gamma)] = \tau_{dis,m}[\Delta r_{m,c}(\gamma)]$, which determines γ.[37,38,43] The mean penetrant hopping time is again computed using Kramers theory,

$$\tau_{hop,p}[\Delta r_p(\gamma)] = \frac{2\tau_{s,p}e^{\beta F_{el,p}(\gamma)}}{d_p^2}\int_{r_{loc,p}}^{r_{loc,p}+\Delta r_p(\gamma)} dr_p e^{\beta F_{dyn,p}(r_p,\gamma)} \times \int_{r_{loc,p}}^{r_p} dr_p' e^{-\beta F_{dyn,p}(r_p',\gamma)}, \tag{15}$$

where $\tau_{s,p} = d_p^2/D_{s,p}$ is the characteristic penetrant short-time scale, given as[37,38,43]

$$\tau_{s,p} = \tau_{E,p}\left[1 + \frac{1}{6\pi^2}\int_0^\infty dqq^2\frac{\rho C_{mp}^2(q)S_{mm}(q)}{1 + \left(d_m^2\tau_{E,p}/d_p^2\tau_{E,m}\right)n(q)/S_{mm}(q)}\right],$$
$$\tau_{E,p} = d_p^2/D_{E,p} = \tau_0\frac{d_p^2d_{mp}^2}{d_m^4}\left(\frac{2m}{m+M}\right)^{1/2}g_{mp}(d_{mp}). \tag{16}$$

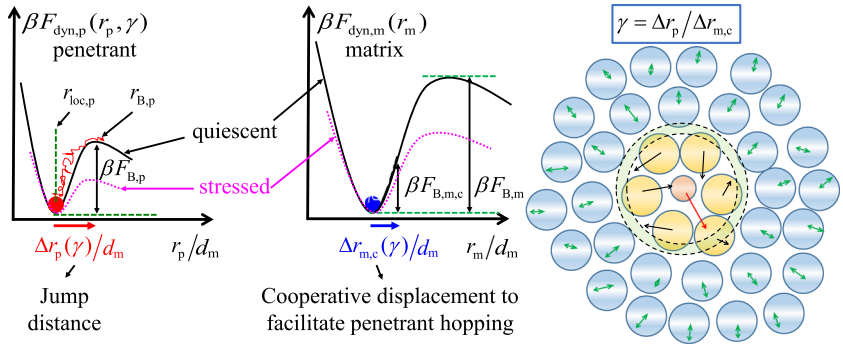

FIG. 3. Key ingredients of the two coupled dynamic free energies under quiescent conditions (black solid curves) in SCCH theory for a single spherical penetrant in a bulk matrix of larger spheres. Trajectory level matrix facilitation of penetrant hopping is formulated based on the concept of a dimensionless coupling parameter, γ, defined as the ratio of the penetrant particle jump distance $\Delta r_p(\gamma)$ to the matrix particle displacement, $\Delta r_{m,c}(\gamma)$. Relevant length and energy scales are indicated. An example of the corresponding dynamic free energy under stress (pink dotted curves) is also shown, which qualitatively indicates how key length and energy scales change relative to the analogs of a quiescent system. The right schematic displays the physical ideas of SCCH theory in the dilute penetrant limit.

Here, $d_{mp} = (d_p + d_m)/2$, where m is the penetrant mass with $m/(m+M) = d_p^3/(d_p^3 + d_m^3)$, $g_{mp}(d_{mp})$ is the contact value of $g_{mp}(r)$, and the penetrant alpha time is the sum of the short-time non-activated process and the activated hopping process contributions, $\tau_{\alpha,p} \equiv \tau_{s,p} + \tau_{hop,p}$. The mean time required for a matrix particle to self-consistently displace a distance $\Delta r_{m,c}(\gamma)$ is denoted as[37,38,43]

$$\tau_{dis,m}[\Delta r_{m,c}(\gamma)] = \frac{2\tau_{s,m} e^{\beta F_{el,m,c}(\gamma)}}{d_m^2} \int_{r_{loc,m}}^{r_{loc,m}+\Delta r_{m,c}(\gamma)} dr_m e^{\beta F_{dyn,m}(r_m)} \times \int_{r_{loc,m}}^{r_m} dr'_m e^{-\beta F_{dyn,m}(r'_m)}. \quad (17)$$

We emphasize that Eqs. (15) and (17) include the elastic barrier contribution in a way that acknowledges that the thermal fluctuation driven motion of the penetrant to its barrier and the coupled facilitating matrix displacement is a *single* time correlated dynamical event. Hence, $F_{el,p} = F_{el,m,c}$, which is given by $\beta F_{el,p} \approx 2\pi r_{cage,p}^3 \Delta r_{eff,p}^2 \rho K_{0,m}$ with $\Delta r_{eff,p}(\gamma) = 3\Delta r_{m,c}^2(\gamma)/32 r_{cage,p}$. This elastic barrier is determined mainly by the matrix dynamic fluctuation distance ($\Delta r_{m,c} = \Delta r_p/\gamma$) and matrix rigidity as encoded in $\rho K_{0,m}$. A previous finding[43] that under quiescent conditions, the contribution from $\Delta r_{m,c} = \Delta r_p/\gamma$ is weak relative to that of $\rho K_{0,m}$ is again found to hold under stress. A strong reduction in both $\Delta r_p/\gamma$ and $\rho K_{0,m}$ with stress suggests a significant decrease in the elastic barrier with the external force. Inserting this elastic barrier into Eqs. (15) and (17), the SCCH theory under external force is then self-consistently constructed.

Figure 3 sketches the conceptual content of SCCH theory for quiescent and stressed conditions based on detailed numerical calculations of the dynamic free energies. In this article, we will not show the many plots of the dynamic free energies and individual quantities derived from them (many are shown in prior studies under quiescent conditions[38,43]) required to analyze the penetrant dynamics problem for the observables of interest. Rather, to keep the article length and number of figures reasonable, we focus on the physically important new predictions that are directly testable in experiments and simulations. This includes the penetrant hopping diffusion constant, which can be crudely calculated from the mean hopping time as $D_p \sim d_p^2/\tau_{hop,p}$.

From our numerical calculations of the dynamic free energies, the following general statements can be made. Under equilibrium conditions, the smaller penetrant is generically less localized and has a lower local cage barrier than its matrix analog. With increasing stress, the penetrant cage barrier decreases more slowly than that of the larger matrix particles because $f_p < f_m$ at the same stress due to the areal prefactor differences in Eqs. (6) and (14). Hence, at a reduced stress rather well below the matrix absolute yield stress, $\beta\sigma_y d_m^3$, the difference between the local cage barriers of the matrix and the penetrant disappears. This signals a crossover to a full "slaving" (maximum coupling) regime where the facilitating matrix dynamic fluctuation (now its structural relaxation event) controls penetrant hopping. The full calculation of the relaxation times requires all relevant aspects of the stress-dependent dynamic free energies per the Kramers formulas given above, including their curvatures at the localization lengths and jump distances, which decrease significantly with increasing stress. These changes result in the prediction that the penetrant elastic barrier associated with the cooperative penetrant–matrix motion decreases significantly with stress even in a nominally low stress ($\sigma/\sigma_y < 0.15$) regime.

B. New questions addressed

The coupled penetrant–matrix activated dynamics under stress for the hard sphere mixture model is characterized by three parameters: stress σ, penetrant-to-matrix size ratio d_p/d_m, and matrix packing fraction ϕ (maps to temperature in a viscous liquid[40,65–67]). How penetrant and matrix relaxation times change as a function of stress in absolute units and relative to a characteristic stress of rheological significance (e.g., yield stress) are of high interest. The remainder of this paper presents new results for the following questions.

Section IV addresses how a specified external stress speeds up the penetrant motion *relative to* the quiescent matrix hopping time. Key questions include: (i) what is the initial functional form and magnitude of stress acceleration of the penetrant hopping time at "low enough" stresses where matrix hopping relaxation is slower than that of the penetrant (decoupling regime) and (ii) what is the crossover stress, σ_c, beyond which slaving emerges. The answers to these questions as a function of size ratio and packing fraction (or, equivalently, quiescent matrix alpha time) are determined. Beyond σ_c, numerical implementation of the full theory predicts that the penetrant and matrix hopping relaxation times are very close. The matrix dynamics under stress have been established in detail by Ghosh and Schweizer[44] and will not be repeated here. We note that based on comparisons to experiment and simulation, the theory[44] successfully predicts a variety of nonlinear rheological phenomena such as stress–acceleration of the alpha relaxation time, elastic modulus softening, steady state flow curve, shear thinning, and yield stress.

Section V studies how decoupling as quantified by the ratio of penetrant-to-matrix alpha relaxation times changes with stress, size ratio, and matrix packing fraction. Subtle aspects arise since stress modifies the penetrant and matrix dynamics in different ways.

The evolution of the absolute values of the penetrant alpha time and transient localization length as a function of control variables is studied is Sec. VI, which is particularly relevant to future experimental and simulation studies of long- and short-time penetrant dynamics under stress. Possible connections between long- and short-time penetrant dynamics and whether connections exist under stress between the penetrant (or matrix) dynamics and the matrix dimensionless compressibility are also studied.

IV. STRESS ACCELERATION AND CROSSOVER TO SLAVED DYNAMICS

We first consider the stress dependence of the penetrant hopping time in units of the matrix quiescent hopping relaxation time. Figure 4(a) shows an example at several matrix packing fractions corresponding to a very wide range of matrix quiescent alpha times. One sees that initially, the penetrant hopping time has a weaker stress dependence than that of the matrix and decreases in a roughly *exponential* manner, which is different from the high power law behavior for the matrix alpha time in Fig. 2(a). Additional calculations in the $\sigma < \sigma_c$ decoupling regime reveal that this is a

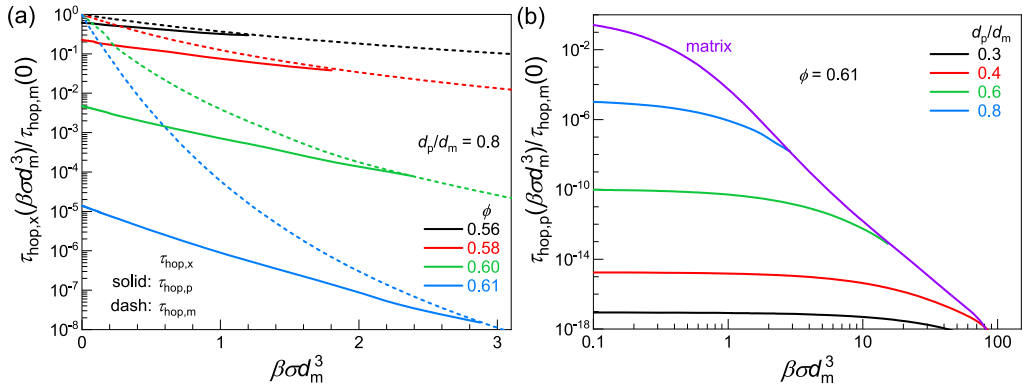

FIG. 4. (a) Penetrant (solid) and matrix (short-dashed) hopping times, normalized by the corresponding *quiescent* matrix hopping time, as a function of scaled stress, $\beta\sigma d_m^3$, plotted in a log-linear manner at a fixed penetrant size ($d_p/d_m = 0.8$) for various matrix packing fractions. The corresponding dimensionless absolute yield stresses for $\phi = 0.56$, 0.58, 0.6, and 0.61 are 33.4, 53.6, 82.2, and 105.9, respectively. (b) Same as in (a) but plotted in a double log format at a fixed packing fraction ($\phi = 0.61$) and various penetrant sizes.

robust trend for all ϕ and d_p/d_m values studied. The reason for the nearly linear decrease in the penetrant total barrier with stress when $\sigma < \sigma_c$ lies in two generic behaviors: (i) dominance of the elastic barrier in the high d_p/d_m regime where stress-induced changes of the penetrant local cage barrier are negligible and (ii) dominance of the local cage barrier in the low d_p/d_m regime where the penetrant elastic barrier is negligible. Figure 12 of the Appendix provides representative quantitative calculations that underlie the above statements concerning the penetrant local cage and collective elastic barriers. Figure 12 also illustrates how the two different barriers respond to stress as a function of penetrant-to-matrix size asymmetry.

We note that if one empirically extrapolated the penetrant hopping time (solid curves in Fig. 4) to beyond σ_c, one might conclude that $\tau_{hop,p} > \tau_{hop,m}$ can weakly occur. However, this would imply that a small-size penetrant surrounded by faster matrix particles relaxes slower than the larger matrix particles, which is not physically intuitive. Indeed, it conflicts with the concept of matrix "constraint or cage release," i.e., $\tau_{hop,p}$ should never be greater than $\tau_{hop,m}$, at the zeroth order. In reality, the issue of relaxation asymmetry as one approaches and exceeds σ_c is technically subtle since it is quantitatively sensitive to prefactors and other second order aspects of the approximate theoretical analysis. For these reasons, we believe that the crossover at $\sigma = \sigma_c$ reflects a regime where matrix activated hopping relaxation starts to control the penetrant hopping time (i.e., when $\tau_{hop,p}$ is very close to $\tau_{hop,m}$). Thus, we adopt, in practice, the physical idea that the penetrant and matrix hopping relaxation times are equal beyond this *a priori predicted* crossover stress.

Figure 4(b) shows the analogous results for various d_p/d_m values at a fixed packing fraction very close to the quiescent matrix glass transition. The onset of slaving begins at a stress that strongly grows as the penetrant size decreases. For small enough penetrants (e.g., $d_p/d_m = 0.3$), no slaving is observed until the matrix absolute yield stress is reached, a consequence of the huge decoupling under quiescent conditions. Nevertheless, for $d_p/d_m = 0.3$, the difference between the penetrant and the matrix hopping relaxation time does decrease significantly with stress.

The slaving onset stress [Fig. 5(a)] is predicted to vary exponentially with size ratio, $\beta\sigma_c d_m^3 \sim \exp(-8.85 d_p/d_m)$, and is largely invariant in form with decreasing packing fraction to within weak deviations at low d_p/d_m. The inset of Fig. 5(a) presents the ϕ-dependence of $\beta\sigma_c d_m^3$ at fixed d_p/d_m. As found for quiescent systems,[43] there is a crossover at $d_p/d_m \sim 0.5$–0.6, beyond which the matrix and penetrant relaxations are strongly coupled in a manner that only modestly weakens with growing packing fraction. In the larger penetrant regime beyond $d_p/d_m \sim 0.5$–0.6, the small amount of quiescent decoupling is destroyed by a very low level of external stress, and the slope of the $\log(\beta\sigma_c d_m^3)$ vs ϕ plot is nearly size ratio independent. These trends explain why there is no packing fraction dependence (to leading order) of the relationship $\beta\sigma_c d_m^3 \sim \exp(-8.85 d_p/d_m)$ in the main frame of Fig. 5(a). Moreover, one also sees that $\beta\sigma_c d_m^3$ increases exponentially with ϕ.

For the smaller penetrant regime that exhibits significant decoupling ($d_p/d_m < 0.5$) in quiescent systems, a threshold stress must be exceeded to significantly reduce the difference between the penetrant and matrix hopping relaxation times. This can be seen in the inset of Fig. 5(a), where $\beta\sigma_c d_m^3$ for the $d_p/d_m = 0.4$ system is much higher than that for larger size ratios. Mechanistically, this higher stress implies that the decrease in the local cage barrier (the elastic barrier is negligible for low d_p/d_m systems; see Fig. 12) cannot be ignored at $\beta\sigma_c d_m^3$, a behavior that differs from when $d_p/d_m > 0.5$, where $\beta\sigma_c d_m^3$ is sufficiently small that any decrease in the local cage barrier can be neglected. These considerations explain why the slope of the $\log(\beta\sigma_c d_m^3)$ vs ϕ plot for $d_p/d_m = 0.4$ in the inset of Fig. 5(a) is larger than that for higher d_p/d_m systems, and why in the main frame of Fig. 5(a) the exponential behavior has the largest (although weak) deviations in the low d_p/d_m regime.

A further comparison between the slaving onset and matrix absolute yield stresses is presented in Fig. 5(b). In contrast to the ϕ-dependence of $\beta\sigma_c d_m^3$ in the high d_p/d_m regime, the theory predicts that $\beta\sigma_y d_m^3$ increases quite strongly with the packing fraction [see the inset of Fig. 1(b)], resulting in a weak *decrease* in the ϕ-dependence of σ_c/σ_y. In contrast, in the low d_p/d_m regime, there is a weak *increase* in the ϕ-dependence of σ_c/σ_y. Despite the

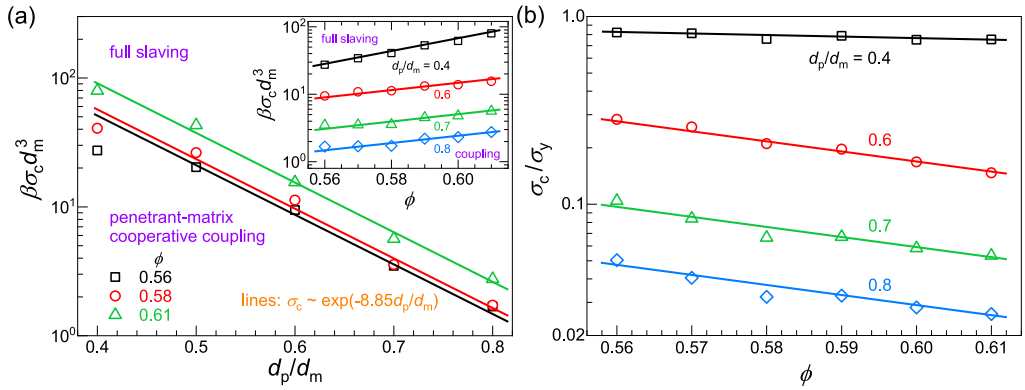

FIG. 5. (a) Dimensionless slaving onset stress (main) as a function of penetrant-to-matrix size ratio for various matrix packing fractions ϕ and (inset) as a function of packing fraction for various size ratios d_p/d_m. (b) Ratio of the slaving onset to matrix absolute yield stresses as a function of packing fraction for various size ratios.

different ϕ-dependent trends in the high and low d_p/d_m regimes, σ_c/σ_y varies exponentially with ϕ for *all* the size ratios studied, since the individual stresses $\beta\sigma_c d_m^3$ and $\beta\sigma_y d_m^3$ both vary exponentially with ϕ. Finally, the penetrant size has a significant influence on σ_c/σ_y due to the pronounced d_p/d_m dependence of $\beta\sigma_c d_m^3$. The latter arises from the sharp increase in the degree of decoupling between the matrix and penetrant dynamics as the size asymmetry ratio decreases.

Figure 4(b) suggests that changing the penetrant size in a fixed ϕ matrix does not directly change the stress dependence of its hopping time, but rather only via the shift of the matrix hopping time due to changes of the slaving onset stress. The results in Fig. 6 confirm this rather dramatic behavior if both axes are normalized by their corresponding values at the slaving onset. A nearly collapsed master curve is predicted *if* the matrix packing fraction is fixed. Thus, from the results in Fig. 6, we deduce that for *all* ϕ and d_p/d_m values studied, there is an exponential relation between the penetrant hopping time and stress when $\sigma < \sigma_c$. In the low d_p/d_m regime, the penetrant elastic barrier is negligible (see Fig. 12), and the local cage barrier determines penetrant relaxation. Hence, the collapse in Fig. 6 is nontrivial because the changes in the local cage barrier at low d_p/d_m and the changes in the elastic barrier at high d_p/d_m conspire to result in a single master curve. This behavior highlights the fundamental connections between the local cage and elastic barriers in the ECNLE theory description of a coupled local–nonlocal activated relaxation event.[39,47,68]

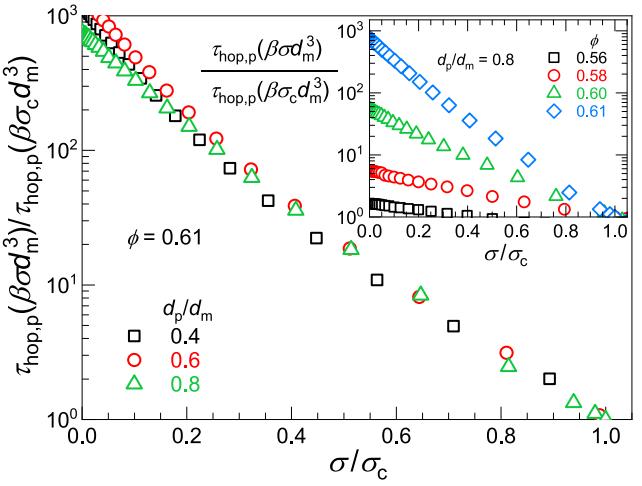

FIG. 6. Penetrant hopping time scaled by its value at the slaving onset stress, $\beta\sigma_c d_m^3$, as a function of σ/σ_c plotted in a log-linear manner at a fixed matrix packing fraction characteristic of the quiescent glass transition ($\phi = 0.61$) for various size ratios d_p/d_m. Inset: same as in the main frame but at a fixed $d_p/d_m = 0.8$ for various matrix packing fractions ϕ.

V. INFLUENCE OF STRESS ON THE DEGREE OF PENETRANT-MATRIX DECOUPLING

The self-consistently determined trajectory coupling parameter γ that enters Eq. (13) controls the amount of real space displacement of the matrix involved in the penetrant activated hopping event. Its value carries mechanistic insight concerning the cooperative "eigenvector" of SCCT theory and the degree of decoupling,[37,38,43] but is not easily determinable in experiment or simulation. Here, we focus on a directly measurable manifestation of decoupling by computing the ratio of the stress-modified penetrant-to-matrix alpha relaxation times, $\tau_{\alpha,p}/\tau_{\alpha,m}$. Slaving corresponds to a value of unity, signaling matrix activated hopping relaxation controls penetrant hopping.

The most interesting regime is at relatively high ϕ (>0.56), where penetrant dynamics (including its decoupling with the matrix) is significantly affected by stress. Figure 7(a) presents the representative decoupling ratio results for a single size ratio. Note that the starting point for these curves (quiescent system) decreases significantly with ϕ, indicating that decoupling increases with the matrix packing fraction. Thus, a larger slaving onset stress is required at a higher ϕ at a fixed penetrant-to-matrix size ratio.

The inset of Fig. 7(a) presents the stress dependence of $\tau_{\alpha,p}/\tau_{\alpha,m}$ for different size ratios. The onset of slaving is shifted to higher stresses for smaller penetrants. However, slaving can disappear

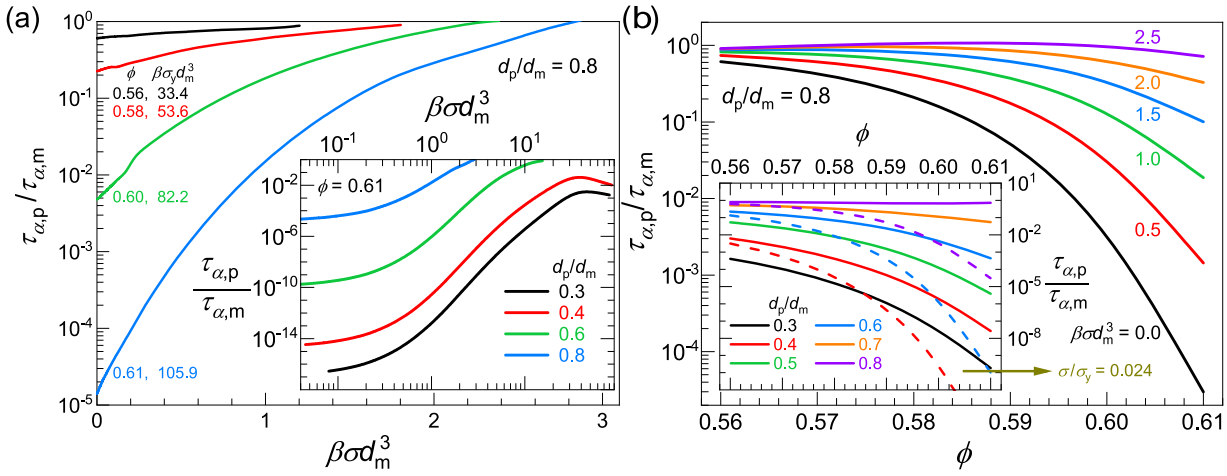

FIG. 7. Degree of decoupling as quantified by the ratio of the stress-dependent penetrant-to-matrix alpha times, $\tau_{\alpha,p}/\tau_{\alpha,m}$. (a) Log-linear plot of $\tau_{\alpha,p}/\tau_{\alpha,m}$ as a function of dimensionless stress at a fixed penetrant-to-matrix size ratio ($d_p/d_m = 0.8$) for four packing fractions. Inset: analogous double log plot at a fixed packing fraction ($\phi = 0.61$) for various d_p/d_m. (b) Log-linear plot of $\tau_{\alpha,p}/\tau_{\alpha,m}$ as a function of packing fraction at a fixed $d_p/d_m = 0.8$ for various scaled stresses, $\beta\sigma d_m^3$. Inset: analogous plot at a fixed low value of σ/σ_y (0.024) for various d_p/d_m; the dashed lines in the inset are the results under quiescent conditions ($\sigma/\sigma_y = 0$).

entirely for low enough values of d_p/d_m. The reason is related to the non-activated short-time scale process since small-size ratios correspond to sufficiently low penetrant cage and elastic barriers that they can become unimportant in determining the total penetrant alpha time. This competition at high stress between the short- and long-time friction explains the weakly non-monotonic decoupling between the penetrant and the matrix in the inset of Fig. 7(a). In Fig. 13 of the Appendix, we present $\tau_{\alpha,p}/\tau_{\alpha,m}$ as a function of d_p/d_m at different values of ϕ and stress. A similar non-monotonic behavior with stress is also predicted for low d_p/d_m in the high stress regime.

Figure 7(b) plots $\tau_{\alpha,p}/\tau_{\alpha,m}$ as a function of ϕ for a fixed d_p/d_m (0.8) at various stresses. One sees that it decreases significantly with increasing ϕ and/or decreasing stress. This is reminiscent of the quiescent system behavior[43] at various size ratios [see also the dashed curves in the inset of Fig. 7(b)], where $\tau_{\alpha,p}/\tau_{\alpha,m}$ decreases significantly with increasing ϕ and/or decreasing d_p/d_m. One can ask how many ways are there to increase the coupling of penetrant and matrix dynamics in the matrix high-density regime and is there an analogous mechanism? Our calculations suggest the answer is as follows: (i) Upon decreasing the matrix packing fraction or increasing stress, the matrix and penetrant total barriers decrease, but the matrix barrier does so *faster* than that of the penetrant, resulting in an *increased* coupling between the matrix and penetrant dynamics. (ii) Upon increasing the penetrant size, both the cage and elastic barriers of the matrix do *not* change. However, in the low d_p/d_m regime, the penetrant local cage barrier increases significantly although its elastic barrier is negligible, while in the high d_p/d_m regime, the penetrant cage barrier remains unchanged, but its elastic barrier increases significantly, as shown in Fig. 12. In either case, an increase in the penetrant *total* barrier then decreases the difference between the matrix and penetrant total barriers, resulting in an increased coupling of their activated dynamics.

The inset of Fig. 7(b) shows the ϕ-dependence of $\tau_{\alpha,p}/\tau_{\alpha,m}$ at various d_p/d_m for a fixed small reduced stress of $\sigma/\sigma_y = 0.024$. This result illustrates that even very far from the matrix absolute yield, stress can significantly modify decoupling. Finally, we note that relative to the influence of packing fraction or stress on the degree of decoupling, penetrant size plays a *more* important role.

VI. INFLUENCE OF STRESS ON THE PACKING FRACTION AND SIZE DEPENDENCES OF PENETRANT DYNAMICS

A. Matrix packing fraction dependence

Increasing the matrix packing fraction is relevant to viscous liquid isothermal high-pressure and isobaric cooling experiments. Two examples of the penetrant alpha relaxation time as a function of packing fraction for a large- and a small-size ratio are shown in Fig. 8(a) at various fixed dimensionless stresses. Beyond the expected decrease in alpha relaxation time with increasing stress, one sees a modest reduction in the rate of increase with packing fraction, although overall, the ϕ-dependence of the penetrant alpha times changes only modestly with stress.

Figure 8(b) shows the analogous plot over a wide range of size ratios at a fixed stress *relative to* the matrix absolute yield stress. This fixed scaled stress constraint reveals how the growth of the penetrant alpha relaxation time with packing fraction changes at a "fixed distance" *far* from the yield point (here, $\sigma/\sigma_y = 0.024$). Since in the low d_p/d_m regime (e.g., 0.4) the local cage barrier dominates the penetrant dynamics and changes only weakly at stresses far from the yield point (see Fig. 12), the effect of stress is weak. However, in the high d_p/d_m regime (e.g., 0.8), both local cage and elastic barriers are crucial for penetrant dynamics, and the high sensitivity of the elastic barrier to even low stresses results in significant changes, which weakens the packing fraction dependence.

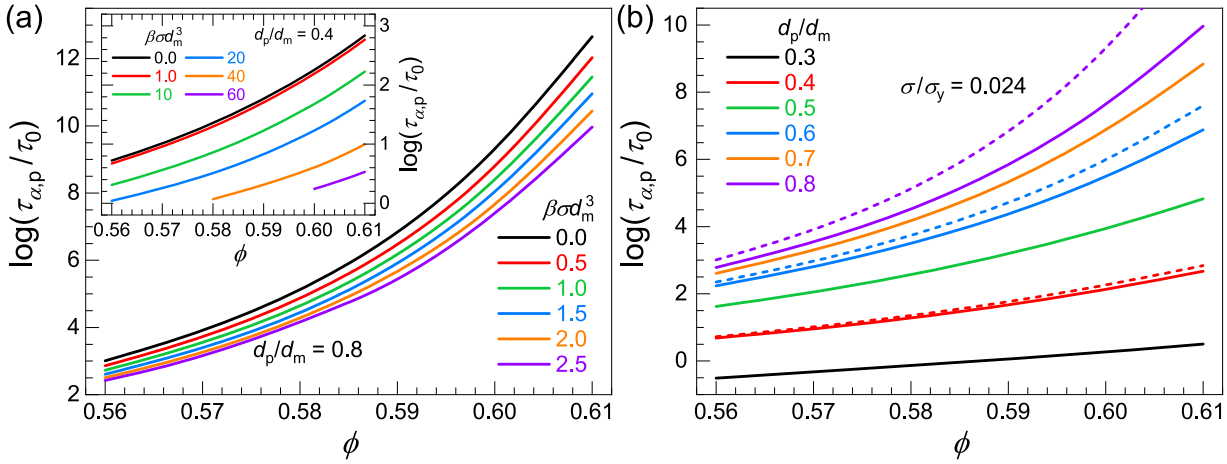

FIG. 8. Logarithm of the penetrant alpha time (unit of the elementary time scale, τ_0) as a function of matrix packing fraction ϕ for (a) various dimensionless stresses at fixed d_p/d_m (0.8 in main, 0.4 in inset) and for (b) various values of d_p/d_m at a fixed low reduced stress σ/σ_y (0.024). Note that the dashed curves are the results under quiescent conditions.

B. Effect of stress on the exponential size ratio dependence of the penetrant alpha time

A striking recent prediction of SCCH theory for quiescent systems is the exponential dependence of the penetrant alpha time on the size ratio,[38,43] which has been confirmed in simulation.[21,69] Its detailed nature depends quantitatively on the matrix packing fraction.[43] Typical results for two packing fractions are shown in Fig. 9. The widest exponential relationship occurs at $\phi = 0.61$ (close to the matrix glass transition), where the penetrant local cage and collective elastic barriers are both important and display compensating variations with size ratio resulting in the total penetrant barrier growing almost linearly with size ratio over the whole range studied (i.e., $0.25 < d_p/d_m < 1.0$).[43]

Figure 9 also shows how stress modifies the exponential relationship between the penetrant alpha time and the size ratio.

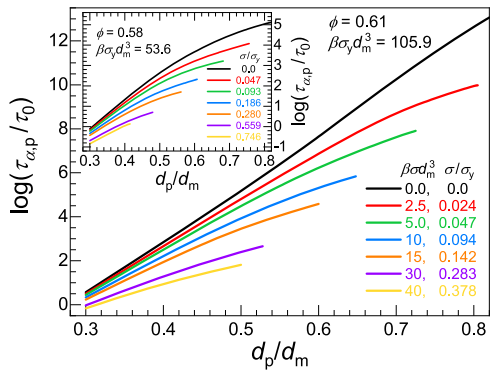

FIG. 9. Logarithm of the penetrant alpha time (in units of τ_0) as a function of size ratio for various values of dimensionless $\beta\sigma d_m^3$ at fixed matrix packing fractions of 0.61 (main plot) and 0.58 (inset). At sufficiently high d_p/d_m, the curves terminate corresponding to the onset of slaving.

Initially, as the size ratio grows, the exponential increase in the penetrant alpha relaxation time still occurs, although the slope and range of its validity monotonically decrease with stress. This trend is qualitatively reminiscent of the behavior of quiescent systems with decreasing packing fraction.[43] Based on Fig. 5(a), beyond a maximum value of d_p/d_m the matrix and penetrant relaxations become slaved, which is the meaning of the termination points of the curves in Fig. 9. Given these results, we expect $\tau_{\alpha,p}/\tau_{\alpha,m}$ will be an exponential function of d_p/d_m to varying degrees with trends per Fig. 9, as confirmed in Fig. 13.

C. Transient dynamic localization length

For equilibrium one-component liquids, ECNLE theory predicts a causal connection between the alpha time and the transient dynamic localization length.[40,47] When extended to the penetrant problem (SCCH theory) under quiescent conditions,[43] the penetrant localization length follows the same connection with the penetrant alpha time. A recent simulation study of penetrants of variable sizes in a cold polymer liquid[21] shows that this localization length is measurable, as it also potentially is based on quasi-elastic neutron scattering measurements that probe the penetrant incoherent dynamic structure factor on local length scales. By confronting the simulated penetrant localization length with its analog in SCCH theory under quiescent conditions,[43] we recently established that it behaves as a power law in the variable d_p/d_m.

We now consider the effect of stress on the above findings. Figure 10 shows that the power law relation between the penetrant localization length and d_p/d_m still applies. Moreover, the apparent power law exponent does not change with stress, and only the absolute value grows modestly. The inset of Fig. 10 shows that the penetrant localization length is predicted to be an exponential function of matrix packing fraction for all size ratios. For the high d_p/d_m regime, because the $\beta\sigma_c d_m^3$ values examined are limited, all the localization lengths for different stresses ($\sigma < \sigma_c$) collapse (results not shown).

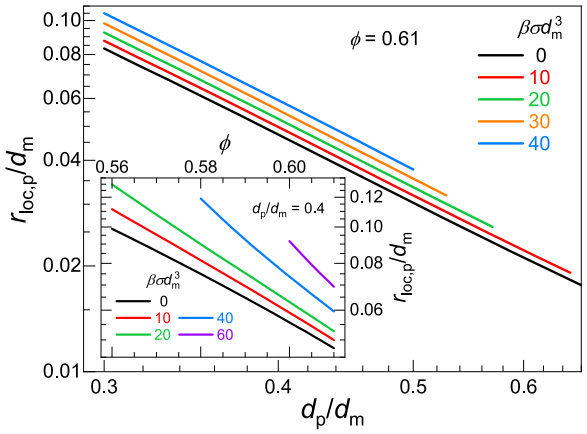

FIG. 10. Localization length (in units of matrix particle diameter, d_m) for various dimensionless stresses as a function of (main) size ratio at ϕ = 0.61 plotted in a double logarithmic manner and (inset) as a function of packing fraction at d_p/d_m = 0.4 in a log-linear manner. The high d_p/d_m termination point of each curve in the main frame corresponds to the onset of slaving.

However, for large enough $\beta\sigma_c d_m^3$ in the lower d_p/d_m regime, one can analyze the validity of the exponential relation over a wide range of stress. An example is shown in the inset of Fig. 10 for d_p/d_m = 0.4, and one sees that the slope grows with stress.

D. Connections between long- and short-time dynamics and thermodynamics

As a matter of equilibrium statistical mechanics, we have previously shown that the matrix inverse dimensionless compressibility, $1/S_0$, grows exponentially with ϕ for a pure hard sphere fluid, i.e., $1/S_0 \sim \exp(C\phi)$, where C is a constant[45] and S_0 is a dimensionless measure of the amplitude of long wavelength thermal density fluctuations of the liquid. Additionally, we have shown that activated relaxation, though causally determined by the local structure in ECNLE theory, is connected with thermodynamics as[47,68] $\log(\tau_{\alpha,m}/\tau_0) \sim \phi r_{loc,m}^{-2} \sim S_0^{-3}$. Here, the first proportionality is dynamically causal, while the second proportionality is *not*, but rather a consequence of the causal *equilibrium* relation between the local pair structure and S_0. From this, one can deduce $r_{loc,m} \sim \exp(-1.5C\phi)$ for the quiescent hard sphere fluid.

For the penetrant problem under quiescent conditions, the SCCH theory predicts[43] (i) a power law relation between the logarithm of the penetrant alpha time and $1/S_0$ with an exponent that varies with penetrant size and (ii) the penetrant effective barrier [i.e., $\log(\tau_{\alpha,m}/\tau_0)$] is directly correlated with its dynamic localization length, analogous to quiescent one-component systems. Thus, the inverse exponential relationship between the penetrant localization length and the matrix packing fraction applies under quiescent conditions. Our new finding here is that these connections persist under stress, although C in $r_{loc,p} \sim \exp(-1.5C\phi)$ increases with d_p/d_m and stress. This suggests that $\log(\tau_\alpha/\tau_0) \sim r_{loc}^{-2} \sim S_0^{-3}$ may also apply to the penetrant alpha times, $\log(\tau_{\alpha,p}/\tau_0) \sim r_{loc,p}^{-2} \sim S_0^{-3}$, even under external stress to within possible stress and size ratio dependent changes of the apparent power law exponent.

For the one-component fluid (matrix in our present study), the relation $\log(\tau_{\alpha,m}/\tau_0) \sim \phi r_{loc,m}^{-2}$ is tested in Fig. 11(a) for various stresses. We find that it remains valid although the slope of the relation decreases with stress. It is well known that the curvature (K_0) of the dynamic free energy at its minimum r_{loc} is an effective spring constant, which is predicted to satisfy $K_0 \sim G' \sim \phi r_{loc}^{-2}$, where G' is the dynamically relaxed plateau shear modulus.[47,68] Thus, the relation $\log(\tau_{\alpha,m}/\tau_0) \sim \phi r_{loc,m}^{-2}$ suggests that a direct linear correlation between the activation barrier (logarithm of the alpha time) and the spring constant also holds out of equilibrium, although

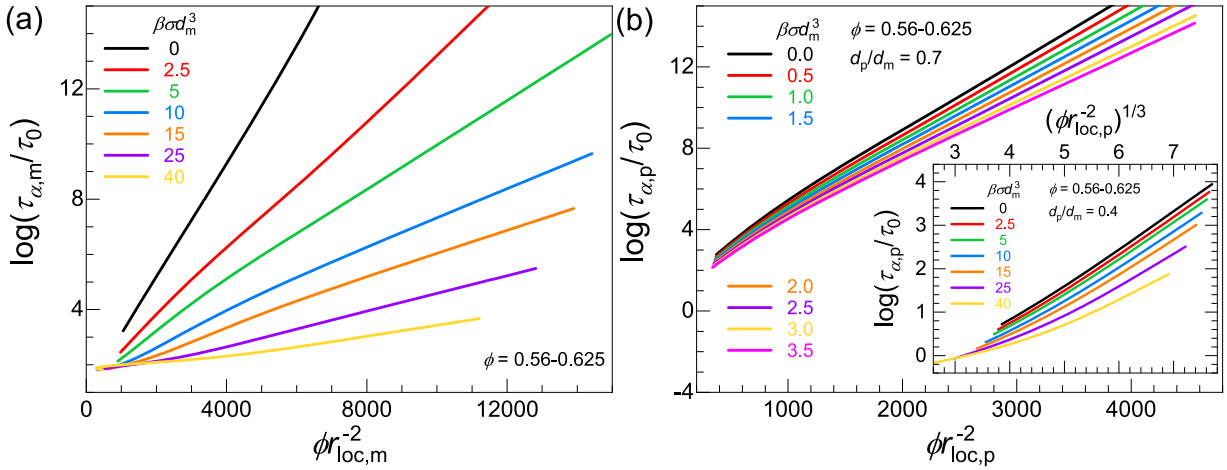

FIG. 11. Relationship between the matrix and penetrant alpha times (in units of τ_0) and their dynamic localization lengths at fixed stress. (a) $\log(\tau_{\alpha,m}/\tau_0)$ vs $\phi r_{loc,m}^{-2}$ for various dimensionless stresses. (b) $\log(\tau_{\alpha,p}/\tau_0)$ vs $\phi r_{loc,p}^{-2}$ for a large-size ratio (d_p/d_m = 0.7) and various values of $\beta\sigma d_m^3 < \beta\sigma_c d_m^3$. Inset: $\log(\tau_{\alpha,p}/\tau_0)$ as a function of $(\phi r_{loc,p}^{-2})^{1/3}$ for a small value of d_p/d_m (0.4) and various values of scaled $\beta\sigma d_m^3 < \beta\sigma_c d_m^3$.

it quantitatively weakens [lower slope of lines in Fig. 11(a)] with stress. Interestingly, these trends appear to be qualitatively identical to the results of a recent work,[70] where it was shown that for driven systems, the stronger the external drive (activity), the weaker is the linear correlation between the alpha relaxation activation barrier and the spring constant (or inverse softness). Finally, we note that by combining $\log(\tau_{\alpha,m}/\tau_0) \sim \phi r_{loc,m}^{-2}$ with $r_{loc,m} \sim \exp(-1.5C\phi)$ and assuming that $1/S_0 \sim \exp(C\phi)$ still applies under external stress, we expect that $\log(\tau_{\alpha,m}/\tau_0) \sim S_0^{-3}$ in a deeply supercooled and/or highly compressed regime continues to apply, as recently discussed for quiescent systems.[43]

Figure 11(b) presents calculations germane to the predicted relationship between the alpha time of a large penetrant ($d_p/d_m = 0.7$) and its corresponding localization length, in analogy to Fig. 11(a) for the pure matrix. As expected, $\log(\tau_{\alpha,p}/\tau_0) \sim \phi r_{loc,p}^{-2}$ still applies under stress, indicating that the so-called compensation effect[43,47] between the penetrant local cage and elastic barriers remains valid for larger penetrants. However, for small penetrants that exhibit much more decoupling from the matrix dynamics, we can deduce based on our previous analysis of quiescent systems[43] that this linear relationship fails since the penetrant elastic barrier is negligible. Rather, a different relationship is now predicted: $\log(\tau_{\alpha,p}/\tau_0) \sim (\phi r_{loc,p}^{-2})^{1/3}$, as confirmed in the inset of Fig. 11(b) for $d_p/d_m = 0.4$, under both quiescent and stressed conditions. Combining these two exponential relationships for large- and small-size ratios and the corresponding localization length results, we find that the cubic (linear) correlation between $\log(\tau_{\alpha,p}/\tau_0)$ and inverse matrix dimensionless compressibility S_0^{-1} in the high (low) d_p/d_m regime is also predicted under stress, as previously found for quiescent conditions.[43]

VII. SUMMARY

We have generalized the microscopic SCCH theory for the activated dynamics of a dilute spherical penetrant or tracer particle in very high-density fluids to include the effect of external stress. The theory was employed to address multiple new questions over a wide range of dimensionless stresses, $\beta\sigma d_m^3$, matrix packing fractions, ϕ, and penetrant-to-matrix particle size ratios, d_p/d_m. The difference between the penetrant and matrix activated hopping times decreases significantly with stress (less decoupling), with a dynamic crossover at a slaving onset stress, $\beta\sigma_c d_m^3$, beyond which the matrix activated hopping relaxation time controls the penetrant hopping time. The slaving onset stress depends sensitively on the matrix packing fraction and size ratio, increases (decreases) exponentially with ϕ (d_p/d_m), and can occur well below the matrix absolute yield stress. These variations are much more sensitive to penetrant size than matrix packing fraction as a consequence of decoupling (as quantified by $\tau_{\alpha,p}/\tau_{\alpha,m}$) in the analogous quiescent systems.

For $\sigma/\sigma_c < 1$, the penetrant hopping time varies exponentially with stress, different from the power law relationship between the pure matrix alpha time and stress.[44] This exponential behavior arises from a linear change in the collective elastic barrier with stress at high d_p/d_m, in contrast to a linear reduction in the local cage barrier with stress at low d_p/d_m. At fixed ϕ, the exponential relations between the penetrant hopping time and stress for different d_p/d_m values can be collapsed onto a master curve if both the penetrant time scale and stress are scaled by their values at the onset of slaving. The ability to construct this master curve reflects nontrivial correlated changes in the local cage and elastic barriers under stress, as previously established under quiescent conditions for both the pure matrix fluid[40,47] and penetrant relaxation problem.[43]

The penetrant transient dynamic localization length under stress is predicted to vary in a power law manner with d_p/d_m, as previously found for quiescent systems.[43] This results in a rather remarkable connection between the short- and long-time penetrant dynamics, qualitatively akin to the situation in one-component fluids,[47] although with the values of some effective exponents depending on size ratio and external stress. Furthermore, (dynamically *noncausal*) connections between the penetrant (or matrix) alpha time and a matrix thermodynamic property, the inverse dimensionless compressibility, are predicted under fixed stress. This is reminiscent of analogous interconnections established both theoretically and experimentally for hard sphere fluids,[43,47] molecular liquids,[68] and inorganic glass formers,[68] albeit with some distinctive differences due to variable coupling between the penetrant and matrix dynamics under stress.

Many of our new predictions for the effect of external stress on penetrant relaxation and diffusivity should be testable in future experimental and simulation studies. Moreover, our results may suggest new practical strategies for controlling penetrant mass transport in membrane separations and other materials science applications. This present work also sets the stage for further generalization to treat multiple real world complications under deformation rich in new physics including thermal liquids under isobaric conditions, nonspherical penetrants, semiflexible polymer chain matrices, and chemical crosslinked polymer networks. Work is underway in these directions.

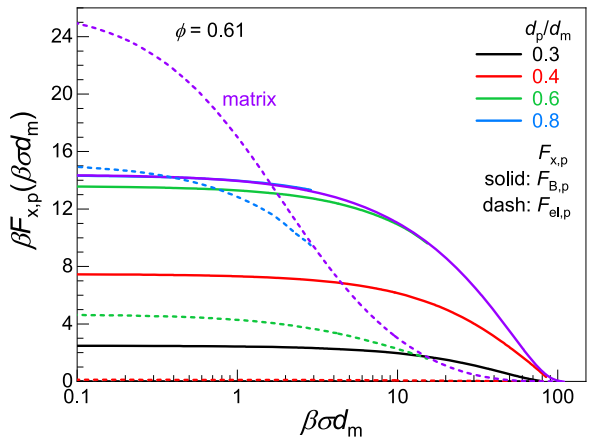

FIG. 12. Penetrant local cage (solid) and collective elastic (short-dashed) barriers in units of thermal energy as a function of scaled stress, $\beta\sigma d_m^3$, plotted in a linear-log format at a fixed high packing fraction ($\phi = 0.61$) for various penetrant sizes ($d_p/d_m = 0.3, 0.4, 0.6, 0.8$). The matrix dimensionless absolute yield stress for $\phi = 0.61$ is 105.9. The corresponding matrix local cage and elastic barriers are also shown (purple curves), and the termination point of each curve for penetrant barriers corresponds to the onset slaving stress σ_c. Lowering of the matrix packing fraction does not change any of the basic behaviors and trends.

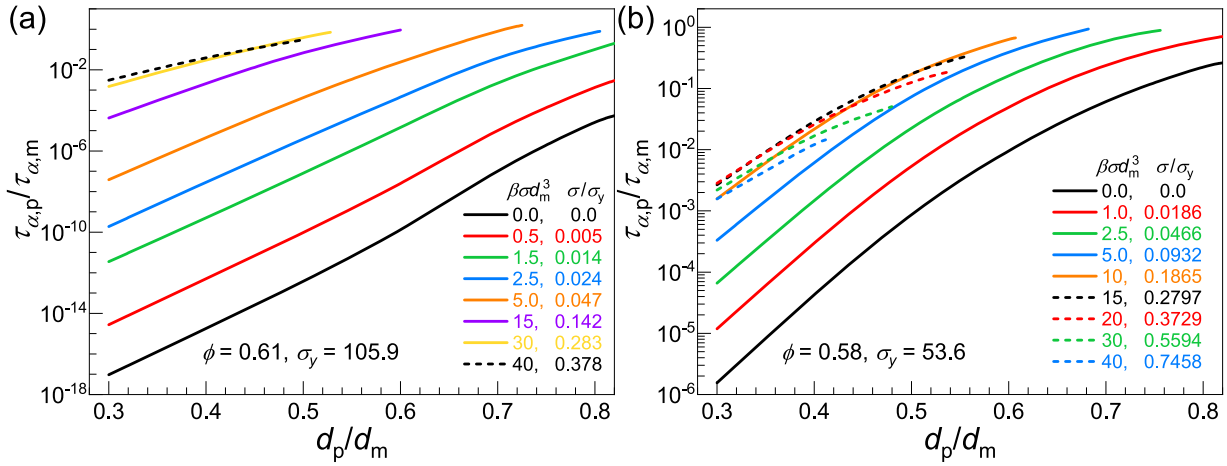

FIG. 13. The decoupling time ratio as a function of penetrant-to-matrix size ratio for various values of dimensionless stress at fixed packing fractions of (a) $\phi = 0.61$ and (b) $\phi = 0.58$.

ACKNOWLEDGMENTS

This research was supported by the U.S. Department of Energy, Office of Basic Energy Sciences, Division of Materials Sciences and Engineering (Award No. DE-SC0020858), through the Materials Research Laboratory at the University of Illinois at Urbana-Champaign. Helpful discussions with Paul Braun, Chris Evans, Randy Ewoldt, and Charles Sing are gratefully acknowledged.

APPENDIX: EFFECT OF STRESS ON PENETRANT BARRIERS AND THE DECOUPLING TIME RATIO

Figure 12 shows the penetrant local cage (solid) and collective elastic (short-dashed) barriers in units of thermal energy as a function of scaled stress, $\beta\sigma d_m^3$, plotted in a linear-log format at a fixed high packing fraction ($\phi = 0.61$) for various penetrant sizes ($d_p/d_m = 0.3, 0.4, 0.6, 0.8$). Figure 13 shows the decoupling time ratio as a function of penetrant-to-matrix size ratio for various values of dimensionless stress at fixed packing fractions of (a) $\phi = 0.61$ and (b) $\phi = 0.58$.

DATA AVAILABILITY

The data that support the findings of this study are available from the corresponding author upon reasonable request.

REFERENCES

[1] K. Paeng, H. Park, D. T. Hoang, and L. J. Kaufman, Proc. Natl. Acad. Sci. U. S. A. **112**, 4952–4957 (2015).
[2] J. Guan, B. Wang, and S. Granick, ACS Nano **8**, 3331–3336 (2014).
[3] S. C. George and S. Thomas, Prog. Polym. Sci. **26**, 985–1017 (2001).
[4] M. T. Cicerone, F. R. Blackburn, and M. D. Ediger, J. Chem. Phys. **102**, 471–479 (1995).
[5] M. Galizia, W. S. Chi, Z. P. Smith, T. C. Merkel, R. W. Baker, and B. D. Freeman, Macromolecules **50**, 7809–7843 (2017).
[6] J. S. Vrentas and C. M. Vrentas, *Diffusion and Mass Transfer* (CRC Press, Boca Raton, 2016).
[7] D. F. Sanders, Z. P. Smith, R. Guo, L. M. Robeson, J. E. McGrath, D. R. Paul, and B. D. Freeman, Polymer **54**, 4729–4761 (2013).
[8] W. J. Koros and R. Mahajan, J. Membr. Sci. **175**, 181–196 (2000).
[9] R. A. May, R. S. Smith, and B. D. Kay, J. Phys. Chem. A **117**, 11881–11889 (2013).
[10] J. Matthiesen, R. S. Smith, and B. D. Kay, J. Chem. Phys. **133**, 174505 (2010).
[11] B. Amsden, Macromolecules **31**, 8382–8395 (1998).
[12] J. N. Ryan and M. Elimelech, Colloids Surf., A **107**, 1–56 (1996).
[13] R. C. Roberts, R. Poling-Skutvik, J. C. Conrad, and J. C. Palmer, J. Chem. Phys. **151**, 194501 (2019).
[14] R. Poling-Skutvik, R. C. Roberts, A. H. Slim, S. Narayanan, R. Krishnamoorti, J. C. Palmer, and J. C. Conrad, J. Phys. Chem. Lett. **10**, 1784–1789 (2019).
[15] E. Martinez-Sotelo, M. A. Escobedo-Sánchez, and M. Laurati, J. Chem. Phys. **151**, 164504 (2019).
[16] E. Lázaro-Lázaro, J. A. Perera-Burgos, P. Laermann, T. Sentjabrskaja, G. Pérez-Ángel, M. Laurati, S. U. Egelhaaf, M. Medina-Noyola, T. Voigtmann, and R. Castañeda-Priego, Phys. Rev. E **99**, 042603 (2019).
[17] R. Higler, R. A. M. Frijns, and J. Sprakel, Langmuir **35**, 5793–5801 (2019).
[18] J. F. Patrick, M. J. Robb, N. R. Sottos, J. S. Moore, and S. R. White, Nature **540**, 363–370 (2016).
[19] B. J. Blaiszik, S. L. B. Kramer, S. C. Olugebefola, J. S. Moore, N. R. Sottos, and S. R. White, Annu. Rev. Mater. Res. **40**, 179–211 (2010).
[20] G. M. Geise, D. R. Paul, and B. D. Freeman, Prog. Polym. Sci. **39**, 1–42 (2014).
[21] M. Kanduč, W. K. Kim, R. Roa, and J. Dzubiella, ACS Nano **15**, 614–624 (2020).
[22] R. Zhang and K. S. Schweizer, Macromolecules **49**, 5727–5739 (2016).
[23] R. Zhang and K. S. Schweizer, J. Chem. Phys. **143**, 144906 (2015).
[24] N. Ramesh, P. K. Davis, J. M. Zielinski, R. P. Danner, and J. L. Duda, J. Polym. Sci., Part B: Polym. Phys. **49**, 1629–1644 (2011).
[25] D. C. Viehman and K. S. Schweizer, J. Chem. Phys. **128**, 084509 (2008).
[26] K. Zhang, D. Meng, F. Müller-Plathe, and S. K. Kumar, Soft Matter **14**, 440–447 (2018).
[27] D. Meng, K. Zhang, and S. K. Kumar, Soft Matter **14**, 4226–4230 (2018).
[28] M. Laurati, T. Sentjabrskaja, J. Ruiz-Franco, S. U. Egelhaaf, and E. Zaccarelli, Phys. Chem. Chem. Phys. **20**, 18630–18638 (2018).
[29] K. Zhang and S. K. Kumar, ACS Macro Lett. **6**, 864–868 (2017).
[30] T. Sentjabrskaja, E. Zaccarelli, C. De Michele, F. Sciortino, P. Tartaglia, T. Voigtmann, S. U. Egelhaaf, and M. Laurati, Nat. Commun. **7**, 11133 (2016).
[31] L. Xi, M. Shah, and B. L. Trout, J. Phys. Chem. B **117**, 3634–3647 (2013).
[32] D. N. Theodorou, "Principles of molecular simulation of gas transport in polymers," in *Materials Science of Membranes for Gas Vapor Separation* (Wiley, Hoboken, NJ, 2006).
[33] J. Budzien, J. D. McCoy, D. Rottach, and J. G. Curro, Polymer **45**, 3923–3932 (2004).
[34] L. Masaro and X. X. Zhu, Prog. Polym. Sci. **24**, 731–775 (1999).

[35] A. A. Gusev, F. Müller-Plathe, W. F. Van Gunsteren, and U. W. Suter, *Atomistic Modeling of Physical Properties* (Springer, 1994), pp. 207–247.
[36] J. S. Vrentas and J. L. Duda, J. Polym. Sci., Part B: Polym. Phys. **15**, 403–416 (1977).
[37] R. Zhang and K. S. Schweizer, J. Phys. Chem. B **122**, 3465–3479 (2018).
[38] R. Zhang and K. S. Schweizer, J. Chem. Phys. **146**, 194906 (2017).
[39] S. Mirigian and K. S. Schweizer, J. Chem. Phys. **140**, 194507 (2014).
[40] S. Mirigian and K. S. Schweizer, J. Chem. Phys. **140**, 194506 (2014).
[41] C. P. Flynn, *Point Defects and Diffusion* (Oxford University Press, Oxford, UK, 1972).
[42] D. Emin, *Polarons* (Cambridge University Press, 2013).
[43] B. Mei and K. S. Schweizer, Soft Matter **17**, 2624–2639 (2021).
[44] A. Ghosh and K. S. Schweizer, J. Chem. Phys. **153**, 194502 (2020).
[45] Y. Zhou, B. Mei, and K. S. Schweizer, Phys. Rev. E **101**, 042121 (2020).
[46] Y. Zhou and K. S. Schweizer, J. Chem. Phys. **150**, 214902 (2019).
[47] B. Mei, Y. Zhou, and K. S. Schweizer, J. Phys. Chem. B **124**, 6121–6131 (2020).
[48] K. S. Schweizer, J. Chem. Phys. **123**, 244501 (2005).
[49] K. S. Schweizer and E. J. Saltzman, J. Chem. Phys. **119**, 1181–1196 (2003).
[50] J.-P. Hansen and I. R. McDonald, *Theory of Simple Liquids* (Elsevier, Amsterdam, 2006).
[51] J. A. Perera-Burgos, J. M. Méndez-Alcaraz, G. Pérez-Ángel, and R. Castañeda-Priego, J. Chem. Phys. **145**, 104905 (2016).
[52] M. Kinoshita, J. Chem. Phys. **118**, 8969–8981 (2003).
[53] L. Verlet, Mol. Phys. **42**, 1291–1302 (1981).
[54] E. J. Saltzman and K. S. Schweizer, J. Chem. Phys. **119**, 1197–1203 (2003).
[55] K. Chen and K. S. Schweizer, Europhys. Lett. **79**, 26006 (2007).
[56] V. Kobelev and K. S. Schweizer, Phys. Rev. E **71**, 021401 (2005).
[57] T. R. Kirkpatrick and P. G. Wolynes, Phys. Rev. A **35**, 3072–3080 (1987).
[58] J. C. Dyre, Rev. Mod. Phys. **78**, 953 (2006).
[59] J. C. Dyre, J. Non-Cryst. Solids **235–237**, 142–149 (1998).
[60] J. C. Dyre, N. B. Olsen, and T. Christensen, Phys. Rev. B **53**, 2171 (1996).
[61] P. Hänggi, P. Talkner, and M. Borkovec, Rev. Mod. Phys. **62**, 251 (1990).
[62] H. A. Kramers, Physica **7**, 284–304 (1940).
[63] E. G. D. Cohen, R. Verberg, and I. M. de Schepper, Physica A **251**, 251–265 (1998).
[64] R. Verberg, I. M. de Schepper, and E. G. D. Cohen, Phys. Rev. E **55**, 3143–3158 (1997).
[65] S.-J. Xie and K. S. Schweizer, Macromolecules **49**, 9655–9664 (2016).
[66] S. Mirigian and K. S. Schweizer, Macromolecules **48**, 1901–1913 (2015).
[67] S. Mirigian and K. S. Schweizer, J. Phys. Chem. Lett. **4**, 3648–3653 (2013).
[68] B. Mei, Y. Zhou, and K. S. Schweizer, Proc. Natl. Acad. Sci. U. S. A. **118**, e2025341118 (2021).
[69] M. Kanduč, W. K. Kim, R. Roa, and J. Dzubiella, Macromolecules **51**, 4853–4864 (2018).
[70] M. K. Nandi and S. M. Bhattacharyya, Phys. Rev. Lett. **126**, 208001 (2021).